High-Resolution Feature Evaluation Benchmark

Kai Cordes, Bodo Rosenhahn, and Jörn Ostermann

Institut für Informationsverarbeitung (TNT)
{cordes,rosenhahn,ostermann}@tnt.uni-hannover.de

Abstract. Benchmark data sets consisting of image pairs and ground truth homographies are used for evaluating fundamental computer vision challenges, such as the detection of image features. The mostly used benchmark provides data with only low resolution images. This paper presents an evaluation benchmark consisting of high resolution images of up to 8 megapixels and highly accurate homographies. State of the art feature detection approaches are evaluated using the new benchmark data. It is shown that existing approaches perform differently on the high resolution data compared to the same images with lower resolution.

1 Introduction

The detection of features is a fundamental step in many computer vision applications. Standing at the beginning of a processing pipeline, the accuracy of such an application is often determined by the accuracy of the detected features. Thus, the development and the evaluation of feature detectors is of high interest in the computer vision community.

The evaluations of feature detectors and descriptors [1,2,3,4,5,6,7] are based on image pairs showing planar scenes and corresponding homographies which determine the mapping between an image pair. This data serves as ground truth for the accuracy evaluation. The mostly used reference data set is proposed by Mikolajczyk et al. [3]. In this set, a sequence consists of 6 images showing the same scene undergoing different types of distortion, such as scale or viewpoint change, illumination, or coding artefacts. The evaluation criterion for feature detectors is the repeatability. The evaluation protocol counts the number of correctly detected feature pairs. A correctly detected feature pair is determined by using a threshold for the overlap error [3]. The threshold controls the demanded accuracy of the evaluation.

The evaluation benchmark [3] has some deficiencies regarding the images as well as the homographies. The image resolution is only 0.5 megapixels. Many images of the data set are not restricted to a plane which is a violation of the homography assumption as shown in Figure 1. For some images, scene content moves between the capturing process (leaves in the *Trees* sequence). It appears that radial distortion is not considered for the benchmark generation which is another violation of the mapping assumption. For the computation of the ground truth homographies, features are used[1]. This is not desirable because the data is used for the evaluation of feature detectors. Finally, the authors concede that the homographies are *not perfect* [8]. However, the data set is used

[1] www.robots.ox.ac.uk/~vgg/research/affine/det_eval_files/DataREADME

R. Wilson et al. (Eds.): CAIP 2013, Part I, LNCS 8047, pp. 327–334, 2013.

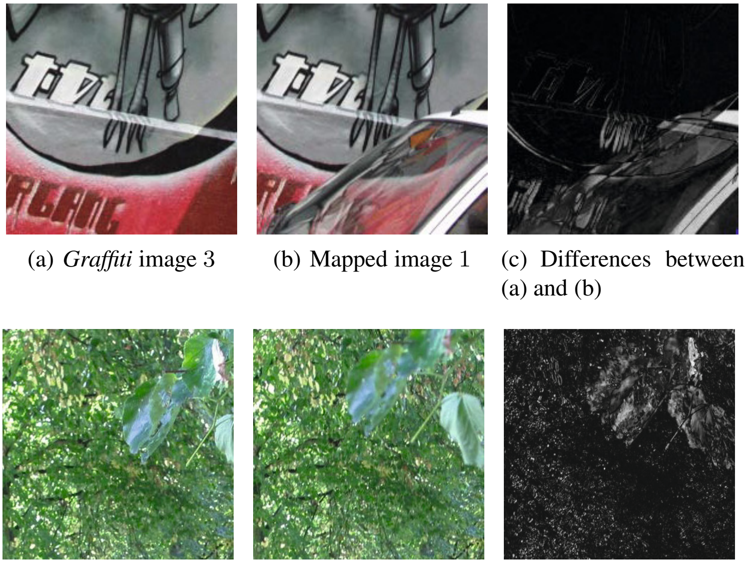

(a) *Graffiti* image 3 (b) Mapped image 1 (c) Differences between (a) and (b)

(d) *Trees* image 3 (e) Mapped image 1 (f) Differences between (d) and (e)

Fig. 1. Part of the mapped images 1 and image 3 of the *Graffiti* sequence (top row) and the *Trees* sequence (bottom row). For the mapping of image 1, the ground truth homographies are used. Large errors occur due to the car in the foreground (*Graffiti*) and the moving leaves because of wind (*Trees*). The bottom part of the *Graffiti* wall indicates a violation of the homography assumption. The error is shown in the images 1(c) and 1(f) (cf. equation (6)).

as ground truth for high-accuracy evaluations, sometimes using very small overlap error thresholds [3,8,9]. Apart from feature evaluation there are applications [10] which use a dense representation of the images. In this case, the mapping errors would spoil the evaluation significantly. Hence, the data set is useless for applications with dense image representations.

Nowadays, consumer cameras provide image resolutions of 8 megapixels or more. The question arises, if feature detector evaluations based on data with 0.5 megapixels are valid for high resolution images. In [3], the evaluated detectors provide scale invariant properties. On the other hand, the localization accuracy of a scale invariant feature may be dependent on the detected scale [11], because its position error in a certain pyramid layer is mapped to the ground plane of the scale space pyramid. In high resolution data, more features are expected to be detected in higher scales of the image pyramid. Thus, a small localization error of a detector may become significant in high resolution image data.

An improved homography benchmark is provided in [12] with image resolutions of 1.5 megapixels per image. In addition, the accuracy of the Mikolajczyk benchmark is slightly increased using a dense image representation instead of image features.

We use the RAW camera data from the images of the data set [12]. The proposed technique exploits the ground truth data from [12] for initializing an evolutionary optimization for the computation of ground truth homographies between image pairs with resolutions of up to 8 megapixels. This technique is called *homography upscaling*. The data is validated using the evaluation protocol invented by [3]. For the comparison between low-resolution and high-resolution benchmark data, the same detectors [3] are evaluated: MSER [13], Hessian-Affine [1], Harris-Affine [8], intensity extrema-based regions (IBR) [14], and edge-based regions (EBR) [15].

The main motivation of this paper is the question if the well known results for the accuracy of feature detectors are still valid for high resolution data. Furthermore, the newly generated high resolution ground truth data set will be provided to the computer vision community for feature detector evaluation or for applications using a dense representation of the images, such as [10].

In the following Section 2, the computation of the new high resolution benchmark is explained. Section 3 shows the accuracy results of the benchmark compared to [12] and the feature evaluation using the repeatability criterion. In Section 4, the paper is concluded.

2 Homography Upscaling

We make use of the RAW image data from [12]. In [12], the benchmark is created using subsampled images of size 1536×1024 (1.5 megapixels). We use the images with the same scene content at higher resolution. The radial distortion is removed in a preprocessing step. Our objective is to create ground truth homographies with image resolutions of up to 3456×2304 (8 megapixels), which is the maximum resolution of the utilized Canon EOS 350D camera.

Since the homography for the image pair at resolution $\mathcal{R}_1$ is approximately known, it can be used for a reasonable initialization for the optimization at resolution $\mathcal{R}_2$ as shown in Section 2.1. The optimization is based on a cost function which computes the mapping error of the homography $\mathtt{H}_{\mathcal{R}_2}$ at resolution $\mathcal{R}_2$. The minimization of the cost function is explained in Section 2.2.

2.1 Upscaling a Homography Analytically

Let the homography between two images at resolution $\mathcal{R}_1 = M_{\mathcal{R}_1} \times N_{\mathcal{R}_1}$ be given as $\mathtt{H}_{\mathcal{R}_1}$. Then, a point $\mathbf{p}_{\mathcal{R}_1}$ of the first image can be identified in the second image with coordinates $\mathbf{p}'_{\mathcal{R}_1}$ by

$$\mathbf{p}'_{\mathcal{R}_1} = \mathtt{H}_{\mathcal{R}_1} \cdot \mathbf{p}_{\mathcal{R}_1} \tag{1}$$

The pixel coordinates of a corresponding image point pair $\mathbf{p}_{\mathcal{R}_1} \leftrightarrow \mathbf{p}'_{\mathcal{R}_1}$ in homogeneous coordinates [16] are normalized to the resolution $\mathcal{R}_0 = [-1; 1] \times [-1; 1]$. This mapping in the left and right image is determined by:

$$\mathbf{p}_{\mathcal{R}_1} = \mathtt{A}_{\mathcal{R}_1} \cdot \mathbf{x}_{\mathcal{R}_0} \quad \text{and} \quad \mathbf{p}'_{\mathcal{R}_1} = \mathtt{A}_{\mathcal{R}_1} \cdot \mathbf{x}'_{\mathcal{R}_0} \tag{2}$$

with the matrix $\mathtt{A}_{\mathcal{R}_1} = \begin{pmatrix} \frac{M_{\mathcal{R}_1}-1}{2} & 0 & \frac{M_{\mathcal{R}_1}-1}{2} \\ 0 & \frac{N_{\mathcal{R}_1}-1}{2} & \frac{N_{\mathcal{R}_1}-1}{2} \\ 0 & 0 & 1 \end{pmatrix}$.

From equations (1) and (2), it follows:

$$\mathtt{A}_{\mathcal{R}_1} \cdot \mathbf{x}'_{\mathcal{R}_0} = \mathtt{H}_{\mathcal{R}_1} \cdot \mathtt{A}_{\mathcal{R}_1} \cdot \mathbf{x}_{\mathcal{R}_0} \tag{3}$$

The desired homography at image resolution $\mathcal{R}_2 = M_{\mathcal{R}_2} \times N_{\mathcal{R}_2}$ is $\mathtt{H}_{\mathcal{R}_2}$. If all image positions from resolutions $\mathcal{R}_1$ and $\mathcal{R}_2$ are normalized to $\mathcal{R}_0$, their coordinates $\mathbf{x}_{\mathcal{R}_0}$ are identical (cf. equations (2)):

$$\mathbf{x}_{\mathcal{R}_0} = \mathtt{A}_{\mathcal{R}_2}^{-1} \cdot \mathbf{p}_{\mathcal{R}_2} \quad \text{and} \quad \mathbf{x}'_{\mathcal{R}_0} = \mathtt{A}_{\mathcal{R}_2}^{-1} \cdot \mathbf{p}'_{\mathcal{R}_2} \tag{4}$$

By exchanging $\mathbf{x}_{\mathcal{R}_0}$ and $\mathbf{x}'_{\mathcal{R}_0}$ in equation (3) with equations (4), it follows:

$$\mathbf{p}'_{\mathcal{R}_2} = \underbrace{\mathtt{A}_{\mathcal{R}_2} \cdot \mathtt{A}_{\mathcal{R}_1}^{-1} \cdot \mathtt{H}_{\mathcal{R}_1} \cdot \mathtt{A}_{\mathcal{R}_1} \cdot \mathtt{A}_{\mathcal{R}_2}^{-1}}_{\mathtt{H}_{\mathcal{R}_2}} \cdot \mathbf{p}_{\mathcal{R}_2} \tag{5}$$

Hence, the homography $\mathtt{H}_{\mathcal{R}_2}$ can be computed by a matrix multiplication consisting of the known matrix $\mathtt{H}_{\mathcal{R}_1}$ and the resolutions $M_{\mathcal{R}_1} \times N_{\mathcal{R}_1}$ and $M_{\mathcal{R}_2} \times N_{\mathcal{R}_2}$ of the left and right image, which build the matrices $\mathtt{A}_{\mathcal{R}_1}$ and $\mathtt{A}_{\mathcal{R}_2}$.

2.2 Optimization Using Differential Evolution

The approximate homography at resolution $\mathcal{R}_2$ is computed from the homography at resolution $\mathcal{R}_1$ as explained in Section 2.1. Due to inaccuracies in $\mathtt{H}_{\mathcal{R}_1}$, the matrix $\mathtt{H}_{\mathcal{R}_2}$ has to be refined by minimizing a cost function. In the following, we denote the homography in the desired resolution with $\mathtt{H} := \mathtt{H}_{\mathcal{R}_2}$. Then, the cost function $E(\mathtt{H})$ is [12]:

$$E(\mathtt{H}) = \frac{1}{J} \sum_{j=1}^{J} d_{\text{RGB}}(\mathtt{H} \cdot \mathbf{p}_j, \mathbf{p}'_j), \tag{6}$$

using the RGB values of the left and the right image $\mathtt{I}_1, \mathtt{I}_2$. The homography $\mathtt{H}$ maps a pixel $\mathbf{p}_j$, $j \in [1; J]$ from the left image $\mathtt{I}_1$ to the corresponding pixel $\mathbf{p}'_j$ in right image $\mathtt{I}_2$. If the homography is accurate, the color distance $d_{\text{RGB}}(\cdot)$ is small. The color distance $d_{\text{RGB}}(\cdot)$ is determined as:

$$d_{\text{RGB}}(\mathbf{p}_i, \mathbf{p}_j) = \frac{1}{3} \cdot (|r(\mathbf{p}_i) - r(\mathbf{p}_j)| + |g(\mathbf{p}_i) - g(\mathbf{p}_j)| + |b(\mathbf{p}_i) - b(\mathbf{p}_j)|) \tag{7}$$

using the RGB values $(r(\mathbf{p}_i), g(\mathbf{p}_i), b(\mathbf{p}_i))$ of an image point $\mathbf{p}_i$. For the extraction of the color values, a bilinear interpolation is used. If a mapped point $\mathbf{p}_j$ falls outside the image boundaries, it is neglected.

Due to lighting and perspective changes between the images, the cost function is likely to have several local minima. Hence, a Differential Evolution (DE) optimizer is used for the minimization of $E(\mathtt{H})$ with respect to $\mathtt{H}$ in the cost function (6). Evolutionary optimization methods have proved impressive performance for parameter estimation challenges finding the global optimum in a parameter space with many local optima. Nevertheless, limiting the parameter space with upper and lower boundaries, increases the performance of these optimization algorithms significantly. For setting the search space boundaries, the approximately known solutions for the homographies at lower resolution are used. With equation (5), the search space centers are computed. Then, a Differential Evolution (DE) optimizer is performed using common parameter settings [17].

3 Experimental Results

For the benchmark generation, 5 sequences are used. Each of the sequences contains 6 images like in the reference benchmark [3]. In Section 3.1, the resulting cost function values of different resolutions are compared. In Section 3.2 the evaluation protocol [3] is performed on the new data.

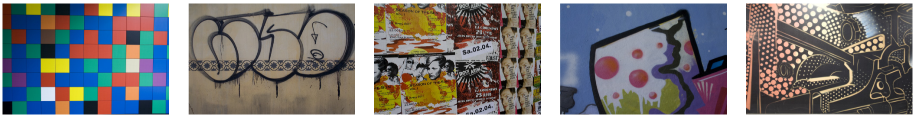

(a) Colors (b) Grace (c) Posters (d) There (e) Underground

Fig. 2. First images of the input image sequences. The resolution is up to 3456×2304.

3.1 High-Resolution Benchmark Generation

The resulting cost function values $E(\mathtt{H})$ for the resolutions $\mathcal{R}_1 = 1536 \times 1024$ and $\mathcal{R}_2 = 3456 \times 2304$ are shown in Table 1. Two example sequences are selected, *Grace* and *Underground*. Due to the high accuracy of the computed homographies at resolution $\mathcal{R}_2$, $E(\mathtt{H})$ increases only slightly compared to resolution $\mathcal{R}_1$. The generally larger error for the *Underground* sequence is due to the higher amount of light reflection from the surface of the wall. Nevertheless, the accuracies of the new homographies are high.

Table 1. Comparison of cost function values $E(\mathtt{H})$ for the homographies for image resolutions 1536×1024 (cf. [12] for *Grace*) and the new data set with resolution 3456×2304. The resulting cost function values for each image pair are approximately the same.

$E(\mathtt{H})$	*Grace*					*Underground*				
	1-2	1-3	1-4	1-5	1-6	1-2	1-3	1-4	1-5	1-6
1.5 megapixels	3.44	4.62	6.02	8.21	9.99	7.23	8.31	12.52	19.07	28.64
8.0 megapixels	3.93	5.20	6.60	8.73	10.46	7.46	8.63	12.67	19.20	28.73

3.2 Repeatability Comparison

To validate the usability of the new data set, the benchmark protocol provided in [3] is used. Like in Section 3.1, we compare results for resolution $\mathcal{R}_1 = 1536 \times 1024$ with $\mathcal{R}_2 = 3456 \times 2304$ for the sequences *Grace* (Figure 4) and *Underground* (Figure 3). Like in the majority of evaluation papers, the overlap error threshold is set to $40\ \%$. The evaluated feature detectors are chosen from the reference paper [3].

Regarding the *Underground* sequence, the results for $\mathcal{R}_2$ are consistent with the results obtained for the smaller resolution $\mathcal{R}_1$. MSER performs best followed by Hessian-Affine and IBR, very similar to the evaluation in [3] for the viewpoint change scenario. But, each of the detectors loose between $1\ \%$ and $9\ \%$ in repeatability.

For the *Grace* sequence, the results are different for each detector. While Harris-Affine and Hessian-Affine perform like in the *Underground* sequence, MSER and IBR

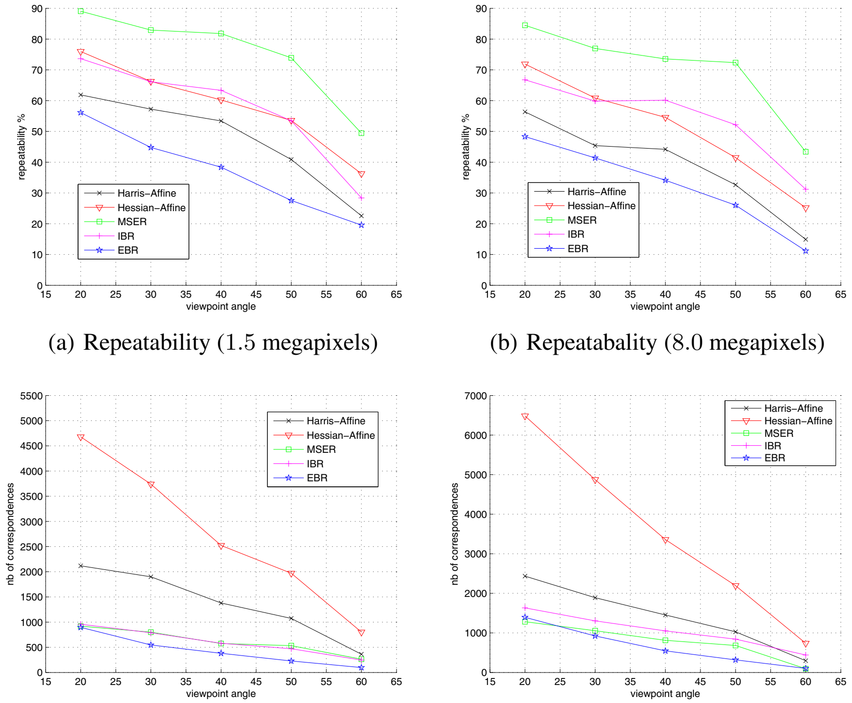

(a) Repeatability (1.5 megapixels)

(b) Repeatabality (8.0 megapixels)

(c) Correspondences (1.5 megapixels)

(d) Correspondences (8.0 megapixels)

Fig. 3. Repeatability results (top row) and the number of correctly detected points (bottom row) for the *Underground* sequence with different resolutions

significantly loose repeatability score. The repeatability rate of IBR decreases between 12 % and 15 % and MSER looses up to 25 % for large viewpoint changes. Interestingly, the EBR gains about 4 % for small viewpoint changes, but looses about 5 % for large viewpoint changes. Generally, none of the detectors can really improve their performance using high resolution images.

4 Conclusions

In this paper, high-resolution image data of up to 8 megapixels is presented together with highly accurate homographies. This data can be used as a benchmark for computer vision tasks, such as feature detection. In contrast to the mainly used benchmark, our data provides high-resolution, fully planar scenes with removed radial distortion and a feature independent computation of the homographies. They are determined by the global optimization of a cost function using a dense representation of the images. The optimization is initialized with values inferred from the solution of lower resolution images.

The evaluation shows that none of the standard feature detection approaches can improve in repeatability on higher resolution images. On the contrary, their performance

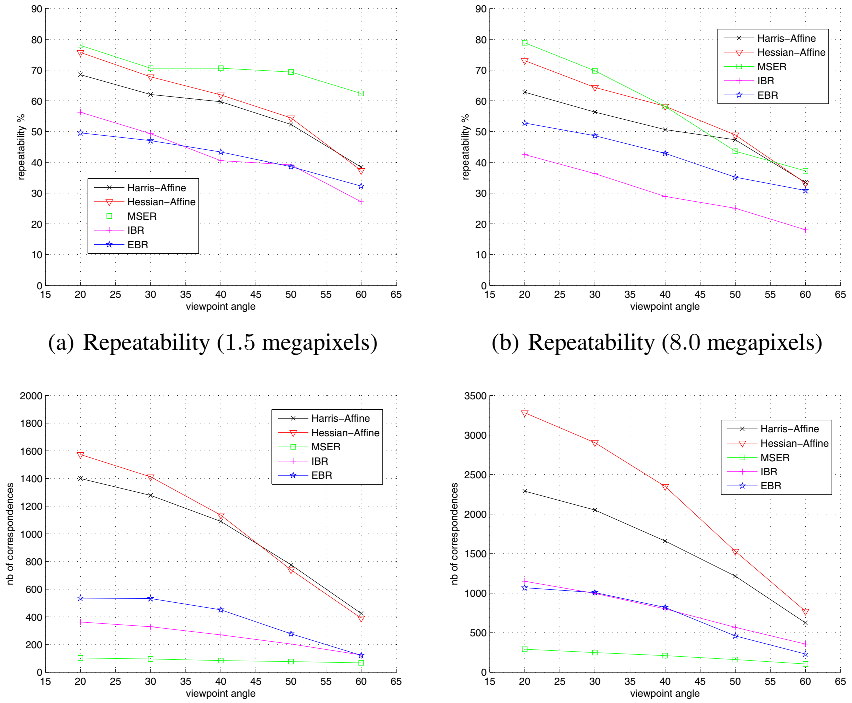

(a) Repeatability (1.5 megapixels)

(b) Repeatability (8.0 megapixels)

(c) Correspondences (1.5 megapixels)

(d) Correspondences (8.0 megapixels)

Fig. 4. Repeatability results (top row) and the number of correctly detected points (bottom row) for the *Grace* sequence with different resolutions

decreases. Dependent on the approach, the repeatability looses up to 25 %, but gains only 4 % in maximum. It follows, that feature detectors should be evaluated using high resolution images. The presented benchmark provides the necessary data to do this.

The data set resulting from this work with all five sequences is available at: `http://www.tnt.uni-hannover.de/project/feature_evaluation/` The provided resolutions include versions with 1.5 megapixels, 3 megapixels, 6 megapixels, and 8 megapixels for each sequence.

References

1. Mikolajczyk, K., Schmid, C.: Scale & affine invariant interest point detectors. International Journal of Computer Vision (IJCV) 60, 63–86 (2004)
2. Mikolajczyk, K., Schmid, C.: A performance evaluation of local descriptors. IEEE Transactions on Pattern Analysis and Machine Intelligence (PAMI) 27, 1615–1630 (2005)
3. Mikolajczyk, K., Tuytelaars, T., Schmid, C., Zisserman, A., Matas, J., Schaffalitzky, F., Kadir, T., Gool, L.V.: A comparison of affine region detectors. International Journal of Computer Vision (IJCV) 65, 43–72 (2005)
4. Schmid, C., Mohr, R., Bauckhage, C.: Comparing and evaluating interest points. In: IEEE International Conference on Computer Vision (ICCV), pp. 230–235 (1998)

5. Schmid, C., Mohr, R., Bauckhage, C.: Evaluation of interest point detectors. International Journal of Computer Vision (IJCV) 37, 151–172 (2000)
6. Haja, A., Jähne, B., Abraham, S.: Localization accuracy of region detectors. In: IEEE Conference on Computer Vision and Pattern Recognition (CVPR), pp. 1–8 (2008)
7. Tuytelaars, T., Mikolajczyk, K.: Local invariant feature detectors: a survey. Foundations and Trends in Computer Graphics and Vision, vol. 3 (2008)
8. Mikolajczyk, K., Schmid, C.: An affine invariant interest point detector. In: Heyden, A., Sparr, G., Nielsen, M., Johansen, P. (eds.) ECCV 2002, Part I. LNCS, vol. 2350, pp. 128–142. Springer, Heidelberg (2002)
9. Förstner, W., Dickscheid, T., Schindler, F.: Detecting interpretable and accurate scale-invariant keypoints. In: IEEE International Conference on Computer Vision (ICCV), Kyoto, Japan, pp. 2256–2263 (2009)
10. Mobahi, H., Zitnick, C., Ma, Y.: Seeing through the blur. In: IEEE Conference on Computer Vision and Pattern Recognition (CVPR), pp. 1736–1743 (2012)
11. Brown, M., Lowe, D.G.: Invariant features from interest point groups. In: British Machine Vision Conference (BMVC), pp. 656–665 (2002)
12. Cordes, K., Rosenhahn, B., Ostermann, J.: Increasing the accuracy of feature evaluation benchmarks using differential evolution. In: IEEE Symposium Series on Computational Intelligence (SSCI) - IEEE Symposium on Differential Evolution (SDE). IEEE Computer Society (2011)
13. Matas, J., Chum, O., Urban, M., Pajdla, T.: Robust wide baseline stereo from maximally stable extremal regions. British Machine Vision Conference (BMVC) 1, 384–393 (2002)
14. Tuytelaars, T., Gool, L.V.: Wide baseline stereo matching based on local, affinely invariant regions. In: British Machine Vision Conference (BMVC), pp. 412–425 (2000)
15. Tuytelaars, T., Van Gool, L.: Content-based image retrieval based on local affinely invariant regions. In: Huijsmans, D.P., Smeulders, A.W.M. (eds.) VISUAL 1999. LNCS, vol. 1614, pp. 493–500. Springer, Heidelberg (1999)
16. Hartley, R.I., Zisserman, A.: Multiple View Geometry, 2nd edn. Cambridge University Press (2003)
17. Price, K.V., Storn, R., Lampinen, J.A.: Differential Evolution - A Practical Approach to Global Optimization. Natural Computing Series. Springer, Berlin (2005)